IOSR Journal of Applied Physics (IOSR-JAP)
e-ISSN: 2278-4861. Volume 5, Issue 5 (Jan. 2014), PP 36-42
www.iosrjournals.org

The electronic band parameters calculated by the Triangular potential model for $Cd_{1-x}Zn_xS$ quantum dot superlattices

S. Marzougui, N. Safta*
Unité de Physique Quantique, Faculté des Sciences, Université de Monastir, Avenue de l'Environnement, 5000 Monastir – Tunisia.

Abstract: *This work reports on theoretical investigation of superlattices based on $Cd_{1-x}Zn_xS$ quantum dots embedded in an insulating material. This system, assumed to a series of flattened cylindrical quantum dots with a finite barrier at the boundary, is studied using the triangular potential. The electronic states and the effective mass of Γ_1 – miniband have been computed as a function of inter-quantum dot separation for different zinc compositions. Calculations have been made for electrons, heavy holes and light holes. Results are discussed and compared with those of the Kronig-Penney and sinusoidal potentials.*
Keywords: *Quantum dots; superlattices; $Cd_{1-x}Zn_xS$; triangular potential; non volatile memories.*

I. Introduction

The potentiality of $Cd_{1-x}Zn_xS$ thin films does not cease to be proved in many device applications especially as window layer material in solar cells based on a conventional p-type absorber layer or quaternary compounds [1 - 10].

As for quantum dots (QDs) based on $Cd_{1-x}Zn_xS$ semiconductor, they are attracting considerable interest in both fundamental and applied research because of their specific properties. In fact, the QDs show a number of striking effects as the quantum confinement, zero-dimensional electronic states and the non linear optical behaviour [6, 11-20]. In epitaxy, also, a progress in the growth of $Cd_{1-x}Zn_xS$ QDs is noted [6, 21-24]. Concerning $Cd_{1-x}Zn_xS$ QDs embedded in a dielectric matrix, they have to be described using spherical model. Based on this geometry, two approaches have been adopted to model the confinement potential, a potential with an infinite barrier [6, 11, 12, 25, 26] and a potential with finite barrier [14, 18] at the boundary. The latter potential permits to predict the coupling between QDs. However, the spherical geometry does not lend simply to calculate the band edges of coupled QDs, particularly along different quantization directions.

In this work, our goal is to investigate the coupling parameters for a chain based on $Cd_{1-x}Zn_xS$ QDs. The confinement potential can be modelled using flattened cylindrical geometry, as reported in Refs [17, 18].

II. Theoretical formulation

In **Fig. 1-a**, we report a schematic diagram of the chain mentioned above. Along a common direction, denoted by z, of spherical $Cd_{1-x}Zn_xS$ QDs, electrons and holes see a succession of flattened cylinders of radius R and effective height L. The inter-quantum dot separation is labelled d which corresponds to the period of the structure. According to that reported in Ref [6], the diameter D = 2R varies from 9 nm to 4 nm going from CdS to ZnS. Thus, if we consider L = 1 nm which corresponds to the value reported in Ref [15], it is evident that L is lower than D and therefore the quantum confinement along transversal direction can be disregarded. Consequently, the $Cd_{1-x}Zn_xS$ multi-quantum dot system can be considered as QDs superlattice (SL) along the longitudinal confined direction. According to this scheme, the system to investigate is a $Cd_{1-x}Zn_xS$ QD superlattice where $Cd_{1-x}Zn_xS$ flattened cylinders behave as quantum wells whereas the host dielectric lattice corresponds to a barrier. For the sake of simplicity, the electron and hole states are assumed to be uncorrelated. Accordingly, the problem to solve is reduced to those of one dimensional potential. In Ref [17], we have adopted the Kronig-Penney model to describe the confinement potential. Using this model, we have calculated the ground and the first excited minibands for both electrons and holes. Calculations were carried out as a function of the ZnS molar fraction and the inter-quantum dot separation. Within this model, we have also computed the longitudinal effective mass versus x and d as well. In Ref [18], we have used the sinusoidal potential to model the confinement of the carriers. Thus, we have studied the ground and the first excited minibands for electrons as a function of inter-quantum dot separation for different zinc compositions. An analysis of the results has evidenced that practically for all the cases studied, the Γ_1 – miniband width of the sinusoidal potential is slightly lower compared to that obtained by the Kronig – Penney model. In this work, we propose the triangular potential to describe the confinement of the carriers. Such a potential can be expressed as:

$$V_{e,h}(z) = \frac{2U_{0e,h}}{\pi}\left|\sin^{-1}\left(\cos\frac{\pi z}{d}\right)\right| \qquad (1)$$

Here $U_{0e,h}$ is the barrier height between adjacent QDs. **Fig. 1-b** shows the shape of this potential energy. Hence, the electron and hole states QDs can be calculated from the Hamiltonien:

$$H_{e,h} = -\frac{\hbar^2}{2m^*_{e,h}}\frac{d^2}{dz^2_{e,h}} + \frac{2U_{0e,h}}{\pi}\left|\sin^{-1}\left(\cos\frac{\pi z_{e,h}}{d}\right)\right| \qquad (2)$$

where $\hbar$ is the Plank's constant, m^* is the effective mass of carriers. The subscripts *e* and *h* refer to electron and hole particles respectively. In deriving the Hamiltonien $H_{e,h}$, we have adopted the effective mass theory (EMT) and the band parabolicity approximation (BPA). The mismatch of the effective mass between the well and the barrier has been disregarded. Values of the electron and hole effective masses for CdS and ZnS are taken from Ref [17]. For $Cd_{1-x}Zn_xS$, these parameters have been calculated using the linear interpolation. The barrier height $U_{0e,h}$ and the inter sheet separation d are treated as parameters. Values of these parameters are taken from Refs [15, 17]. Table.1 reports parameters used to calculate the Γ_1 − miniband for $Cd_{1-x}Zn_xS$ QD superlattices.

III. Results

In a first step, by solving the Schrodinger equation corresponding to the Hamiltonien $H_{e,h}$, we have calculated, for electrons, the width ΔE_{1e} of Γ_1 −miniband as a function of the inter-quantum dot separation. Typical results are depicted in Fig 2. In addition, these results were fitted by polynomial laws as a function of d for the different compositions studied and summarized in Table.2. Some peculiar features were revealed: (i) the Γ_1 − miniband width shows a decreasing tendency with increased ZnS molar fraction independently to the inter-QD separation. For $Cd_{1-x}Zn_xS$ QDs with low zinc contents, the order of magnitude of the width ΔE_{1e} is important and shows the strong degree of coupling between the QDs. At high zinc compositions, however, ΔE_{1e} is lower. Since the effective mass m^*_e remains practically unchanged for all Zn compositions, this result is, presumably related to the barrier potential height U_{0e}. Indeed, this parameter is found to increase with x [15] (ii) for any composition x, the width ΔE_{1e} of the Γ_1 −miniband decreases with the increase of the SL period d. The difference between the Γ_1 −miniband widths for CdS QDs is equal to 0.24 eV while that of the ZnS-related QDs is of 0.14 eV. For intermediate compositions, this difference is ranged between the two extreme values. For $Cd_{1-x}Zn_xS$ QDs with low zinc contents, the coupling between nanoparticles shows a significant drop as the inter – quantum dot separation increases. This behaviour can be attributed to the low potential barrier heights. Thus, the high coupling is governed by the tunnelling effect for shorter SL periods. But for larger inter-QD separations, the tunnelling effect becomes weaker even if the barrier heights are low. However, for larger ZnS molar fractions, the coupling is practically independent of d. Such a trend is due mainly to the largeness of barrier heights.

For comparison with results obtained by using the Kronig-Penney and the sinusoidal potential models [17, 18], we report in Table.3, widths of Γ_1 − miniband as calculated in the present work and those obtained in Refs. [17, 18]. As can be seen, for low and intermediate Zn compositions, the Γ_1 − miniband widths of this work are slightly lower. For high zinc compositions, however, the Γ_1 − miniband widths of this work are globally slightly higher. Therefore, one can conclude that, contrarily to the high zinc compositions range, the triangular potential does not account for the coupling as much as than the Kronig-Penney and the sinusoidal potentials in the cases of low and intermediate zinc contents. This result can be explained in terms of barrier height value. Indeed the latter becomes large at high zinc compositions.

In a second step, we have calculated, for the heavy holes and light holes, the Γ_1 − miniband width. This parameter is denoted for these carriers by ΔE_{1hh} and ΔE_{1lh} respectively. Calculations were also carried out for the Zn compositions and inter-sheet separations studied. The results are depicted in Fig.3.b and Fig.3.c.

Compared with that related to electrons, one can note that: (i) both ΔE_{1hh} and ΔE_{1lh} increase with increased Zn composition independently to the inter-QD separation. This result is mainly due to the fact that, for heavy holes and light holes, the effective mass decreases as a function of composition x (ii) contrarily to ΔE_{1hh}, ΔE_{1lh} is slightly lower than ΔE_{1e}. As a consequence, the superlattice behavior affects not only the conduction electrons but also the light holes especially for short SL periods. This result can be attributed to the difference in effective masses between the electrons and light holes on the one hand and the heavy holes on the other hand.
Let us now focus our interest on the longitudinal dispersion relation of the SL structures based on $Cd_{1-x}Zn_xS$ QDs. This relation shows the k-dependence of minibands along the [001] direction. Fig. 4 depicts, for electrons, the k_z – dependent energy of Γ_1 −miniband for CdS and ZnS QD systems. As can be seen from the plots, the dispersion of this miniband is superior for CdS, compared with that related to ZnS QDs. Furthermore, this dispersion is found to decrease going from CdS to ZnS. Also discussed in this paper is the longitudinal electron effective mass m^*_{e,Γ_1} for the $Cd_{1-x}Zn_xS$ QDs studied. In order to deduce this parameter we consider a parabolic line to the miniband dispersion at the vicinity of the minima. The longitudinal effective masses have been calculated for the Γ_1 −miniband from the second derivative of the band energy with respect to the wave vector k_z. All the effective masses are expressed in units of the free electron mass m_0. Calculations have been made as a function of inter-quantum dot separation for Zn compositions studied. Results are summarized in Tables 4 and 5. An analysis of these results revealed that: (i) the electron mass m^*_{e,Γ_1} increases with the ZnS molar fraction for any SL period (ii) for $Cd_{1-x}Zn_xS$ QDs with low zinc contents, one can observe that the SL period does not significantly affect the electron effective mass. In these conditions, electrons can move easily through the SL structures (iii) for $Cd_{1-x}Zn_xS$ QDs with intermediate zinc compositions, however, the mobility of electrons becomes lower than that of the first composition range (iv) for high zinc compositions, the electron effective mass in the Γ_1 − miniband is higher even for short SL periods. In this composition range, the mobility of electrons is significantly affected for any inter-quantum dot separation and therefore the QDs can be considered as isolated. On the other hand, it is worth to notice that when d is superior to 2.5 nm, the effective mass being related to the miniband dispersion cannot be defined in the case of intermediate and high zinc compositions. For $Cd_{1-x}Zn_xS$ QDs with low zinc contents, however, the effective mass m^*_{e,Γ_1} is well defined when d is superior to 2.5 nm. Nevertheless, this parameter is, in the last case, rather higher in such a way that the electron mobility becomes difficult.

For the holes, the same procedure has been adopted to calculate the longitudinal effective mass. Table.6 shows the obtained results. As a consequence, the mobility of heavy holes is insignificant in terms of magnitude order. This result confirms the strong localization character of these carriers. As for light holes, the mobility is, globally, not far from the one of the electrons. The last result is in agreement with the fact that $Cd_{1-x}Zn_xS$ QDs are appropriate to form superlattice behavior for the electrons and light holes.

IV. Conclusion

We investigated the electronic properties of nanostructure based on $Cd_{1-x}Zn_xS$ embedded in a dielectric matrix for compositions ranging from CdS to ZnS. To describe the QDs, we have adopted the flattened cylindrical geometry with a finite potential barrier at the boundary. Using the triangular potential model, we have calculated, in a first step, the Γ_1 −miniband for electrons, heavy holes and light holes. Calculations have been made as a function of inter-quantum dot separation for different Zn compositions. For electrons, an analysis of the results has evidenced that: (i) the widths of Γ_1 − miniband decrease as the ZnS molar fraction increases (ii) for a given Zn composition, the miniband width decreases with increased inter-quantum dot separation. For heavy holes, the Γ_1 −miniband is shown to be significantly lower in comparison with the electron miniband. This reflects the strong localization character of the heavy holes in the $Cd_{1-x}Zn_xS$ nanostructures. For light holes, however, the Γ_1 −miniband widths are slightly lower than those related to electrons. $Cd_{1-x}Zn_xS$ QDs are appropriate to give rise a superlattice behavior for both electrons and light holes especially for short SL periods. A comparison of results concerning the electrons revealed that contrarily to the high zinc compositions range, the triangular potential does not account for the coupling as much as than the Kronig-Penney and the sinusoidal potentials in the cases of low and intermediate zinc contents. From the SL band structure, as calculated for $Cd_{1-x}Zn_xS$ QDs, we have derived, in a second step, for electrons, heavy holes and light holes the longitudinal effective mass versus x and d as well. The obtained results reveal that the

mobility is insignificant in terms of magnitude order for the heavy holes. For the light holes, however, values of this parameter are not far from those of the electrons. In the applied physics, this study is of great interest for designing a new class of nanocrystal devices based on $Cd_{1-x}Zn_xS$ QDs particularly the non – volatile memories.

Acknowledgements

The authors are very grateful to Mr Houcine Ghalla Doctor in "Unité de Physique Quantique, Faculté des Sciences, Université de Monastir" for his precious help.

References

[1] H. Hu, H. Shen, C. Cui, D. Liang, P. Li, S. Xu, W. Tang, J. Alloys Compd. 560 (2013) 1-5.
[2] N.A. Noor, N. Ikram, S. Ali, S. Nazir, S.M. Alay-e-Abbas, A. Shaukat, J. Alloys Compd. 507 (2010) 356–363.
[3] A. Sakly, N. Safta and A. Ben Lamine, Journal of materials Science-Materials in electronic, 15 (2004) 351-354
[4] N. A. Shah, A. Nazir, W. Mahmood, W. A. A. Syed, S. Butt, Z. Ali and A. Maqsood, J. Alloys Compd. 512 (2012) 27-32.
[5] T. P. Kumar, S. Saravanakumar and K. Sankaranayanan, Appl. Surf. Sci. 257 (2011) 1923-1927.
[6] B. Bhattacharjee, S. K. Mandal, K. Chakrabarti, D. Ganguli and S. Chaudhui, J. Phys. D: Appl. Phys. 35 (2002) 2636-2642.
[7] H.H. Gürel, Ö. Akinci and H. Ünlü, Thin Solid Films 516 (2008) 7098-7104.
[8] M. Gunasekaram, M. Ichimura, Sol. Energy Mater. Sol. Cells. 91 (2007) 774-778.
[9] N. Gawedang, T. Gawedang, Materials Letters, 59 (2005) 3577
[10] J. Lee, W. Song and J. Yi, Thin Solid Films 431-432 (2003) 349.
[11] K.K Nanda, S.N. Sarangi, S. Mohanty, S.N. Sahu, Thin Solid Films 322 (1998) 21-27.
[12] H. Yükselici, P. D. Persans and T. M. Hayes, Phys. Rev. B. 52 (1995) 11763.
[13] Y. Kayanuma, Phys. Rev. B 38 (1988) 9797
[14] N. Safta, A. Sakly, H. Mejri and Y. Bouazra, Eur. Phys. J. B 51 (2006) 75-78
[15] N. Safta, A. Sakly, H. Mejri and M. A. Zaïdi, Eur. Phys. J. B 53 (2006) 35 – 38
[16] A. Sakly, N. Safta, A. Mejri, H. Mejri, A. Ben Lamine, J. Nanomater (2010), ID746520.
[17] A. Sakly, N. Safta, H. Mejri, A. Ben Lamine, J. Alloys Compd. 476 (2009) 648–652.
[18] A. Sakly, N. Safta, H. Mejri, A. Ben Lamine, J. Alloys Compd.509 (2011) 2493–2495
[19] L Zhou, Y Xing and Z P Wang, Eur. Phys. J. B. 85 (2012) 212
[20] A. John Peter and C. W. Lee, Chinese Phys. B 21 (2012) 087302
[21] L Cao, S Huang and S. E J. colloid Interface Sci. 273 (2004) 478.
[22] H. Kumano, A. Ueta and I. Suemune, Physica E 13 (2002) 441-445.
[23] Y. Cai Zhang, W. Wei Chen and X. Ya Hu, Materials Letters 61 (2007) 4847-4850.
[24] K. Tomihira, D. Kim and M. Nakayama, J. Lumin.112 (2005) 131-135.
[25] Q. Pang, B.C. Guo, C.L. Yang, S. H. Yang, M.L. Gong, W.K. Ge and J. N. Wang, Journal of Crystal Growth, 269 (2004) 213.
[26] M.C. Klein, F. hache, D. Ricard and C. Flytzanis, Phys Rev. B. 42 (1990) 11123.

Table. 1 Parameters used to calculate the Γ_{1e} - , Γ_{1hh} - and Γ_{1lh} - minibands for $Cd_{1-x}Zn_xS$ QD superlattices.

x	$\frac{m_e^*}{m_0}$	$\frac{m_{hh}^*}{m_0}$	$\frac{m_{lh}^*}{m_0}$	U_{0e} (eV)	U_{0h} (eV)	$L\ (nm)$
0.0	0.16	5.00	0.70	0.10	0.25	1.0
0.2				0.25	0.25	1.0
0.4				0.45	0.50	1.0
0.6				0.75	0.50	1.0
0.8				1.50	0.50	1.0
1.0	0.28	1.76	0.23	2.00	2.00	1.0

Table. 2 The fit of the calculated electron effective masses (in units of m_0) versus d for different Zn compositions

Composition x en zinc	*Polynomial law*
0.0	$2.22 - 2.37d + 0.96d^2 - 0.14d^3$
0.2	$1.85 - 1.78d + 0.65d^2 - 0.08d^3$
0.4	$1.99 - 2.14d + 0.84d^2 - 0.11d^3$
0.6	$1.61 - 0.169d + 0.65d^2 - 0.09d^3$
0.8	$1.62 - 1.76d + 0.71d^2 - 0.10d^3$
1.0	$0.96 - 0.18d + 0.25d^2 - 0.02d^3$

Table. 3 Widths of the Γ_1 (eV) –miniband for the present work (a) and those obtained by the kronig-penney potential (b) and the sinusoidal potential (c).

d (nm) x	1.5	1.7	1.9	2.1	2.3	2.5
0.0	0.369[(a)]	0.286[(a)]	0.240[(a)]	0.210[(a)]	0.150[(a)]	0.130[(a)]
	0.727[(b)]	0.586[(b)]	0.468[(b)]	0.370[(b)]	0.312[(b)]	0.267[(b)]
	0.710[(c)]	0.520[(c)]	0.449[(c)]	0.345[(c)]	0.276[(c)]	0.230[(c)]
0.2	0.320[(a)]	0.251[(a)]	0.200[(a)]	0.163[(a)]	0.136[(a)]	0.115[(a)]
	0.676[(b)]	0.533[(b)]	0.408[(b)]	0.306[(b)]	0.250[(b)]	0.216[(b)]
	0.587[(c)]	0.450[(c)]	0.335[(c)]	0.281[(c)]	0.226[(c)]	0.190[(c)]
0.4	0.289[(a)]	0.224[(a)]	0.173[(a)]	0.145[(a)]	0.120[(a)]	0.101[(a)]
	0.586[(b)]	0.442[(b)]	0.306[(b)]	0.234[(b)]	0.175[(b)]	0.153[(b)]
	0.511[(c)]	0.379[(c)]	0.292[(c)]	0.223[(c)]	0.178[(c)]	0.136[(c)]
0.6	0.254[(a)]	0.198[(a)]	0.158[(a)]	0.130[(a)]	0.108[(a)]	0.009[(a)]
	0.494[(b)]	0.335[(b)]	0.242[(b)]	0.153[(b)]	0.112[(b)]	0.075[(b)]
	0.420[(c)]	0.307[(c)]	0.230[(c)]	0.165[(c)]	0.120[(c)]	0.085[(c)]
0.8	0.236[(a)]	0.184[(a)]	0.146[(a)]	0.120[(a)]	0.100[(a)]	0.080[(a)]
	0.331[(b)]	0.191[(b)]	0.102[(b)]	0.065[(b)]	0.037[(b)]	0.025[(b)]
	0.229[(c)]	0.148[(c)]	0.091[(c)]	0.064[(c)]	0.044[(c)]	0.023[(c)]
1.0	0.210[(a)]	0.163[(a)]	0.131[(a)]	0.107[(a)]	0.080[(a)]	0.070[(a)]
	0.234[(b)]	0.130[(b)]	0.051[(b)]	0.039[(b)]	0.012[(b)]	0.012[(b)]
	0.162[(c)]	0.105[(c)]	0.055[(c)]	0.034[(c)]	0.023[(c)]	0.009[(c)]

Table.4 The longitudinal electron effective masses m^*_{e,Γ_1} (in units of m_0) as a function of the inter-sheet separation for $Cd_{1-x}Zn_xS$ QD superlattices.

d (nm) x	1.5	1.7	1.9	2.1	2.3	2.5
0.0	0.1990	0.1993	0.1996	0.2000	0.2004	0.2010
0.2	0.2157	0.2179	0.2194	0.2213	0.2237	0.2315
0.4	0.2343	0.2375	0.2430	0.2487	0.2568	0.2719
0.6	0.2572	0.2694	0.2861	0.3083	0.3381	0.4332
0.8	0.3118	0.3692	0.4576	0.5951	0.8022	0.9082
1.0	0.3776	0.5012	0.7095	1.0599	1.6549	1.7869

Table.5 The fit of the calculated electron effective masses (in units of m_0) versus the inter-QD separation for different Zn compositions.

Zinc composition x	Γ_{1e} - Miniband
0.0	$0.193+0.001d-0.004d^2+2.314*10^{-4}d^3$
0.2	$0.123+0.137d-0.069d^2+0.012d^3$
0.4	$0.246-0.028d+0.011d^2+0.001d^3$
0.6	$0.144+0.169d-0.111d^2+0.032d^3$
0.8	$-1.096+2.538d-1.669d^2+0.402d^3$
1.0	$-6.253+12.007d-7.556d^2+1.665d^3$

Table.6 The longitudinal hole effective masses m^*_{hh,Γ_1} (a) and m^*_{lh,Γ_1} (b) (in units of m_0) calculated as a function of the inter-sheet separation for $Cd_{1-x}Z_nS$ QD superlattices.

d (nm) x	1.5	1.7	1.9	2.1	2.3	2.5

0.0	6.0750[(a)]	6.0754[(a)]	6.0763[(a)]	6.0775[(a)]	6.0801[(a)]	6.0840[(a)]
	0.8929[(b)]	0.8936[(b)]	0.8943[(b)]	0.8950[(b)]	0. 8957[(b)]	0.8964[(b)]
0.2	5.1902[(a)]	5.1922[(a)]	5.1960[(a)]	5.2014[(a)]	5.2102[(a)]	5.2225[(a)]
	0.7311[(b)]	0.7334[(b)]	0.7353[(b)]	0.7374[(b)]	0.7399[(b)]	0.7421[(b)]
0.4	4.4691[(a)]	4.4985[(a)]	4.5922[(a)]	4.7136[(a)]	5.0255[(a)]	5.1284[(a)]
	0.6276[(b)]	0.6498[(b)]	0.6709[(b)]	0.6918[(b)]	0.7120[(b)]	0.7323[(b)]
0.6	3.6854[(a)]	3.7190[(a)]	3.8085[(a)]	3.9482[(a)]	4.1792[(a)]	4.5165[(a)]
	0.5040[(b)]	0.5190[(b)]	0.5472[(b)]	0. 5780[(b)]	0.6052[(b)]	0.6394[(b)]
0.8	2.9030[(a)]	2.9584[(a)]	3.0501[(a)]	3.4969[(a)]	3.8982[(a)]	4.0325[(a)]
	0.3891[(b)]	0.4092[(b)]	0.4297[(b)]	0.4536[(b)]	0.4793[(b)]	0.4989[(b)]
1.0	2.1014[(a)]	2.1522[(a)]	2.3037[(a)]	2.5786[(a)]	3.1948[(a)]	3.9438[(a)]
	0.2734[(b)]	0.2891[(b)]	0. 3097[(b)]	0.3295[(b)]	0.3592[(b)]	0.3795[(b)]

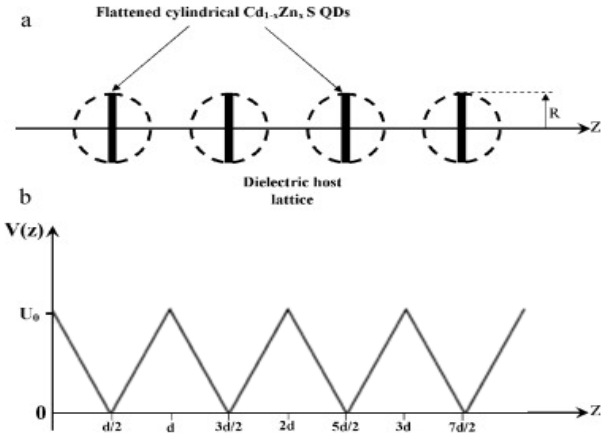

Figure.1 (a) A schematic diagram of $Cd_{1-x}Zn_xS$ QD superlattices according to the flattened cylindrical geometry – (b) The triangular potential used in this work.

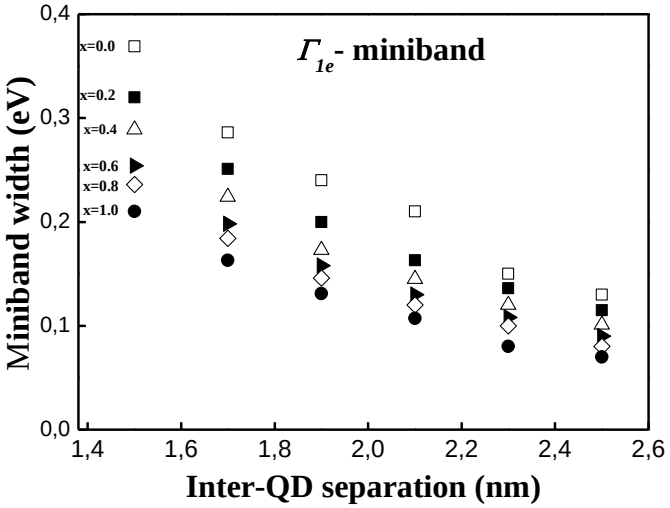

Figure.2 The Γ_1 – miniband width, as calculated for electrons versus the inter-QD separation for different Zn compositions.

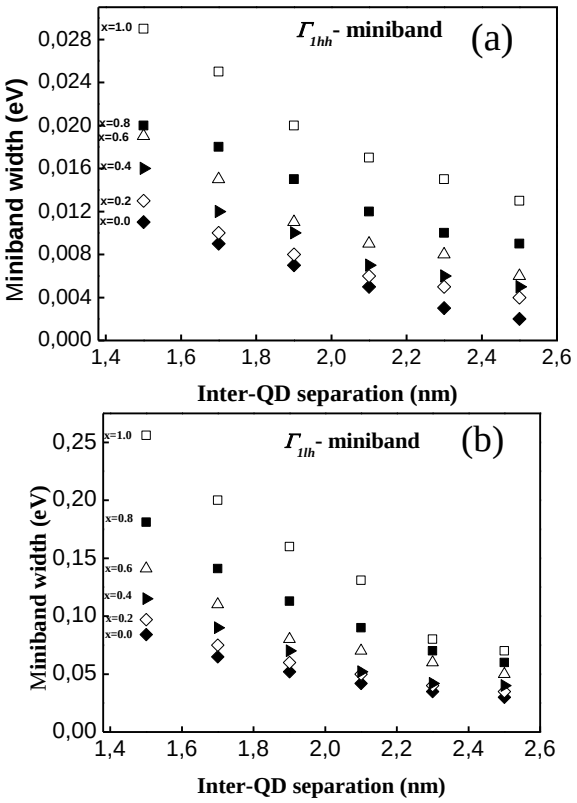

Figure.3 The Γ_1 − miniband width, as calculated for heavy holes (a) and light holes (b) versus the inter-QD separation for different Zn compositions.

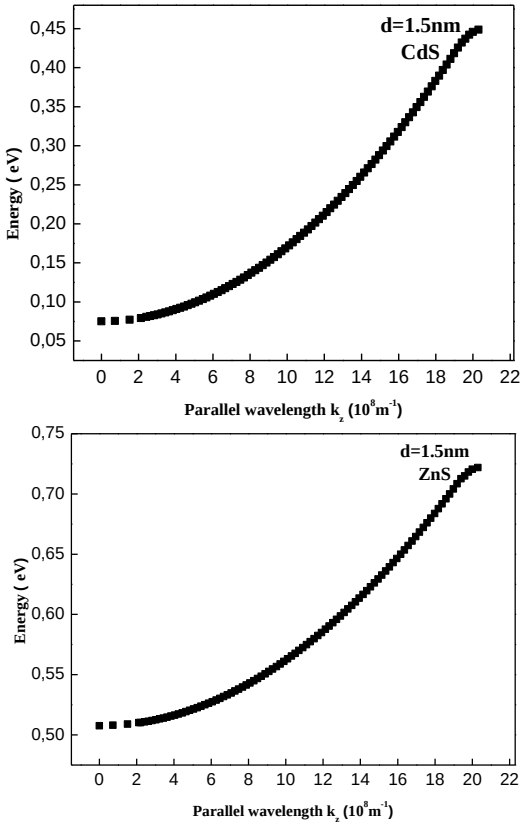

Figure.4 The k_z – dependent energy of Γ_1 − miniband for CdS and ZnS QD systems.